Supersonic Turbulent Boundary Layer in Adverse Pressure Gradient. Part II: Data Analysis

WALTER B. STUREK*
Ballistic Research Laboratories, Aberdeen Proving Ground, Md.
AND
JAMES E. DANBERG†
University of Delaware, Newark, Del.

Experimental measurements of the mean profile characteristics of the supersonic turbulent boundary layer in a moderate adverse pressure gradient are analyzed. Turbulent boundary-layer equations applicable to compressible flow over a surface with longitudinal curvature are evaluated by numerical integration using the tabulated profile data. Curvature corrections to the equation for conservation of streamwise momentum are shown to be small but of the same order of magnitude as the wall shear stress. The data are shown to correlate in law of the wall dimentionless coordinates using an integral compressibility transformation that follows directly from Prandtl's mixing length approximation of the Reynolds stress. Values of skin-friction coefficient determined using the experimental data are compared to other experimental data and to values predicted using the Spalding-Chi method.

Nomenclature

c_f = skin-friction coefficient
C = law of the wall constant
K = constant in Prandtl's mixing length relation $l = Ky$
M = Mach number
p = pressure
R = local radius of longitudinal curvature
Re_θ = momentum thickness Reynolds number
T = temperature
$U = u + u'$ = velocity in the streamwise direction
u_τ = friction velocity, $(\tau_w/\rho_w)^{1/2}$
u^{++} = transformed dimensionless velocity, defined by Eq. (12)
$V = v + v'$ = velocity normal to the local surface
x = streamwise distance
y = distance normal to the local surface
y^+ = dimensionless distance normal to the local surface, $u_\tau y/\nu_w$
β = curvature correction factor, $1/(1+\kappa y)$
δ = boundary-layer thickness
δ^* = boundary-layer displacement thickness
δ_u = boundary-layer velocity thickness
θ = boundary-layer momentum thickness
θ_E = boundary-layer energy thickness
θ_H = boundary-layer enthalpy thickness
κ = inverse longitudinal curvature
ρ = density
τ = shear stress
Π = Cole's wake parameter

Subscripts

aw = adiabatic wall
o = supply header condition
t = local stagnation condition
w = property evaluated at the wall
δ = property evaluated at $y = \delta$
∞ = reference condition, property evaluated external to the boundary layer for $dp/dx = 0$ and at $y = \delta$ for $dp/dx > 0$

Superscripts

$( )'$ = indicates "ideal" property, calculated using measured p, constant $p_t = p_o$ and $T_t = T_{t\infty}$; also used to indicate fluctuation component

Introduction

THIS paper consists of an extensive analysis of the experimental data reported in Ref. 1. The objectives of this analysis are 1) evaluate the quality of the experimental data and 2) contribute to the basic understanding of the supersonic turbulent boundary layer in an adverse pressure gradient.

Analysis

Equations of Conservation of Mass and Momentum

Considerable experimental evidence has been shown in Ref. 1 in the form of profiles of the mean properties (Mach number, mass flux, temperature) showing distinct differences in the profile shapes between the zero pressure gradient and the adverse pressure gradient flows. It is obvious that the boundary-layer equations as applicable to the flow over the ramp model must contain terms that include the effects of the pressure gradient

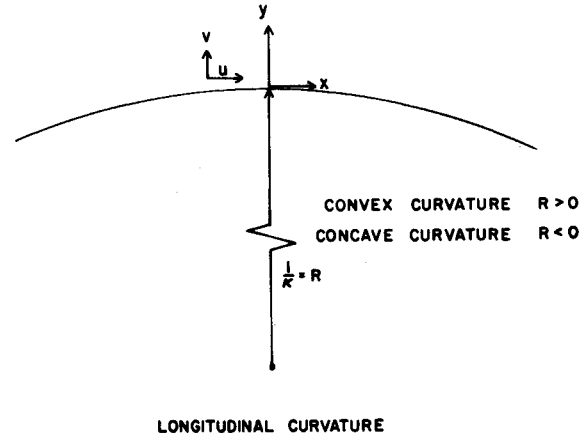

Fig. 1 Coordinate system for longitudinal surface curvature.

Presented as Paper 71-162 at the 9th Aerospace Sciences Meeting, New York, January 25–27, 1971; submitted July 28, 1971; revision received November 22, 1971.
Index categories: Boundary Layers and Convective Heat Transfer—Turbulent; Supersonic and Hypersonic Flow.
* Aerospace Engineer. Member AIAA.
† Associate Professor, Department of Mechanical and Aerospace Engineering. Member AIAA.

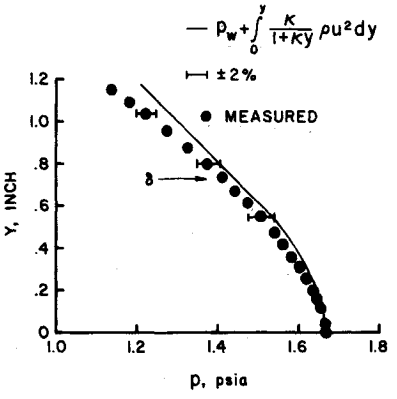

Fig. 2 Static pressure profile, measurement compared with calculation.

normal to the model surface, pressure gradient in the streamwise direction and the curvature of the surface.

Tetervin[2] has derived the conservation equations in a form applicable to the compressible turbulent boundary layer over a surface with both longitudinal and transverse curvature. The coordinate system is illustrated in Fig. 1. The equations were derived by considering the continuity equation and the Navier-Stokes equations in their most general form. The usual assumption that the instantaneous turbulent density, velocity and pressure can be represented by the sum of a mean component plus a fluctuating component is introduced, and the flow is considered to be restricted to one in which

$$\begin{aligned} \partial/\partial y,\ \kappa &= 0\,(1/\delta) & v &= 0\,(\delta) \\ \rho, u, T, \partial/\partial x &= 0\,(1) & \mu &= 0\,(\delta^2) \\ \rho', u', v', T' &= 0\,(\delta^{1/2}) & \mu' &= 0\,(\delta^{5/2}) \end{aligned}$$

By considering only a two-dimensional steady mean flow over a surface with longitudinal curvature the following system of equation is obtained.

Conservation of Mass

$$\partial(\rho u)/\partial x + \partial[(1+\kappa y)(\rho v + \langle \rho' v' \rangle)]/\partial y = 0 \tag{1}$$

Conservation of Momentum

$$\begin{aligned} &[1/(1+\kappa y)]\rho u(\partial u/\partial x) + (\rho v + \langle \rho' v' \rangle)(\partial u/\partial y) + (\rho v + \langle \rho' v' \rangle) \times \\ &\quad u[\kappa/(1+\kappa y)] = -[1/(1+\kappa y)](\partial p/\partial x) + \partial(\mu u - \rho \langle u' v' \rangle)/\partial y + \\ &\quad [2\kappa/(1+\kappa y)][\mu(\partial u/\partial y) - \rho \langle u' v' \rangle] - [\kappa/(1+\kappa y)][\partial(\mu u)/\partial y] - \\ &\qquad \mu u(\kappa/1+\kappa y)^2 \end{aligned} \tag{2}$$

$$(\rho/2)\partial(\langle v'^2 \rangle + \langle w'^2 \rangle)/\partial y - [\kappa/(1+\kappa y)](\rho u^2 + 2u \langle \rho' u' \rangle + \rho \langle u'^2 \rangle) = -(\partial p/\partial y) \tag{3}$$

In order to apply this system of equations to the flow over the ramp model, κ is assigned the 0(1). This scales all length dimensions with respect to R. The actual physical scaling, δ/R, is approximately 0.02 for the flow over the ramp model. Retaining terms of 0(1) in Eqs. (1, 2 and 3), we find

Conservation of Mass

$$\partial(\rho u)/\partial x + \partial[(1+\kappa y)(\rho v + \langle \rho' v' \rangle)]/\partial y = 0 \tag{4}$$

Conservation of Momentum

$$\begin{aligned} &[1/(1+\kappa y)]\rho u(\partial u/\partial x) + (\rho v + \langle \rho' v' \rangle)(\partial u/\partial y) = \\ &\quad -[1/(1+\kappa y)](\partial p/\partial x) + \partial[\mu(\partial u/\partial y) - \rho \langle u' v' \rangle]/\partial y \end{aligned} \tag{5}$$

$$(\rho/2)\partial(\langle v'^2 \rangle + \langle w'^2 \rangle)/\partial y - [\kappa/(1+\kappa y)]\rho u^2 = -(\partial p/\partial y) \tag{6}$$

The importance of including terms arising from the longitudinal curvature in Eqs. (4, 5 and 6) will now be examined by numerical integration using the tabulated profile data.

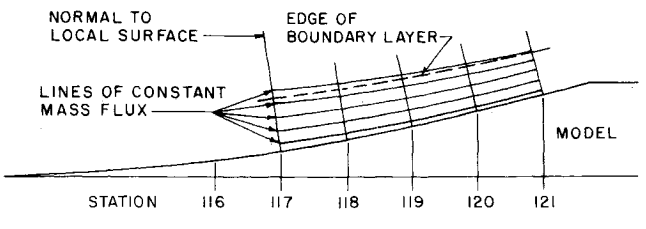

Fig. 3 Lines of constant mass flux.

Conservation of Mass

Integration Eq. (4) in the y direction yields

$$(1+\kappa y)(\rho v + \langle \rho' v' \rangle) = -\int_0^y \frac{\partial}{\partial x}(\rho u)\, dy \tag{7}$$

Longitudinal curvature enters this calculation only as the factor $(1+\kappa y)$ which is approximately 0.98 at $y = \delta$ for this experiment. Hence, the mass flux in the y direction at $y = \delta$ is increased approximately 2% by longitudinal curvature over the integral of the partial derivative of the streamwise mass flux.

Conservation of Momentum Normal to the Surface

Since the fluctuation terms in Eq. (6) were not measured in this experiment, the equation for the conservation of momentum in the y direction will be considered in the following form.

$$[\kappa/(1+\kappa y)]\rho u^2 = \partial p/\partial y \tag{8}$$

This equation can be written in integrated form as

$$p(y) = p_w + \int_0^y \frac{\kappa}{1+\kappa y}\rho u^2\, dy \tag{9}$$

A typical static pressure profile obtained by numerical integration of Eq. (9) is shown in Fig. 2 compared to the measured profile. The bars indicate an uncertainty of ±2% about the measured value. The trend indicated by both profiles is in agreement throughout the boundary layer. The profiles agree within +0 and −2% within the boundary layer, but greater divergence is indicated beyond the edge of the boundary layer.

Conservation of Streamwise Momentum

Combining Eqs. (4) and (5), integrating in the y direction across the boundary layer and using Leibnitz's formula for differentiation of integrals yields

$$\begin{aligned} &\frac{d}{dx}\int_0^\delta \beta\rho u^2\, dy - u_\infty \beta_\delta \frac{d}{dx}\int_0^\delta \rho u\, dy - \\ &\quad \int_0^\delta u\left[\int_0^y \frac{\partial}{\partial x}(\rho u)\, dy\right]\beta^2\kappa\, dy + \frac{d}{dx}\int_0^\delta \beta p\, dy - \beta_\delta p_\delta \frac{d\delta}{dx} = -\tau_w \end{aligned} \tag{10}$$

where $\beta = 1/(1+\kappa y)$ and $\tau = \mu\,\partial u/\partial y - \rho \langle u' v' \rangle$.

The numerical integration of the first, second and fourth terms on the LHS is easily accomplished. The third term, however, requires knowledge of the quantity $\partial(\rho u)/\partial x$ as a function of position through the boundary layer. This quantity has been evaluated along lines of constant mass flux using a least squares technique. An example showing the trend of the lines of constant mass flux is shown in Fig. 3 compared with the trend of the boundary-layer thickness. It is obvious that even though the boundary layer is becoming less thick, mass is being entrained within the boundary layer. An example of the distribution of $\partial(\rho u)/\partial x$ is shown in Fig. 4.

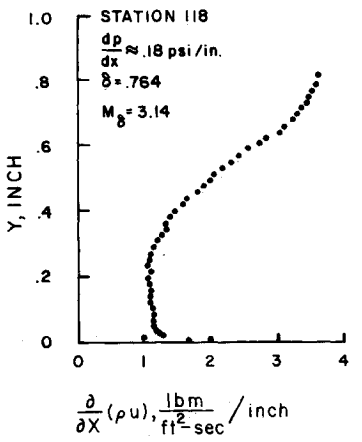

Fig. 4 The distribution of $\partial(\rho u)/\partial x$.

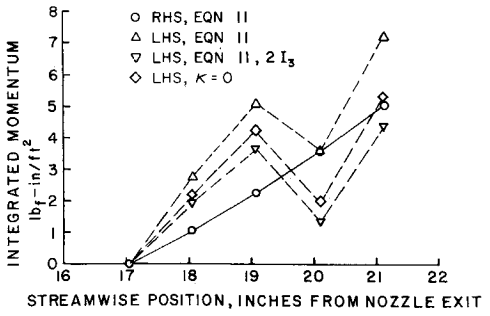

Fig. 5 Streamwise integrated balance of momentum.

Values of the first and fourth integrals in Eq. (10) with and without the curvature correction are tabulated for comparison in Table 1. The effect of concave longitudinal curvature is to increase the value of the integral. For this flow configuration, this effect is seen to be less than 1.5%. These calculations indicate that the corrections for longitudinal curvature are small; however as will be shown, are of the same order of magnitude or larger than the wall shear stress. In this respect the curvature corrections are significant.

A more discriminating appraisal of the effect of including corrections for longitudinal curvature can be made by considering the balance of streamwise integrated momentum.

By making the following substitutions

$$I_1 = \int_0^\delta \beta\rho u^2\,dy; \qquad I_2 = \int_0^\delta \rho u\,dy; \qquad I_4 = \int_0^\delta \beta p\,dy$$

$$I_3 = \int_0^\delta u\left[\int_0^y \frac{\partial}{\partial x}(\rho u)\,dy\right]\beta^2\kappa\,dy$$

into Eq. (10) and integrating the resulting expression in the streamwise direction, the following relation for the streamwise integrated balance of momentum is obtained.

$$\int_a^b dI_1 - \int_a^b u_\infty \beta_\delta\, dI_2 - \int_a^b I_3\,dx + \int_a^b dI_4 - \int_a^b \beta_\delta p_\delta\, d\delta = -\int_a^b \tau_w\,dx \qquad (11)$$

Equation (11) has been evaluated numerically from station to station. An example of this calculation is tabulated in Table 2 where the individual terms in Eq. (11) are numbered consecutively starting on the left.

The result of these calculations is best evaluated by plotting the LHS of Eq. (11) vs streamwise position. This plot is shown in Fig. 5 compared to the RHS. Also shown for comparison is the result obtained upon setting $\kappa = 0$. The data appear to be consistent through Station 119; however, an inconsistency is indicated at Station 120. No reason for this discrepancy has been identified in the profile data.

Table 1 Comparison of integral terms with and without corrections for longitudinal curvature

Sta	$\int_0^\delta \rho u^2\,dy$ lbf-in./ft²	$\int_0^\delta \beta\rho u^2\,dy$ lbf-in./ft²	$\int_0^\delta p\,dy$ lbf-in./ft²	$\int_0^\delta \beta p\,dy$ lbf-in./ft²
117	1054.97	1070.45	139.4	140.9
118	1101.43	1117.06	152.8	154.4
119	1125.73	1141.02	165.0	166.7
120	1157.86	1169.70	177.2	178.7
121	1198.79	1213.61	192.1	193.9

The agreement shown between the LHS and the RHS of Eq. (11) is seen to be within +2.5% of the largest term (T_2). Surprisingly enough, better agreement is indicated when the curvature correction is neglected. Values of the terms in Eq. (2) which were later dropped as a result of the order of magnitude analysis have been evaluated, and the last term on the LHS of Eq. (2) was found to provide a significant contribution. Including this term results in I_3 being multiplied by 2. The result of including this term is also shown in Fig. 5. It is seen that the agreement with the integrated wall shear stress is improved.

It should be emphasized that in evaluating the LHS of Eq. (11) the difference is taken between very large numbers to yield an answer that is approximately 0.3% of the largest term. This implies that the experimental profiles must be extremely accurate to achieve good agreement. Evaluation of the streamwise integrated momentum provides a very discriminating check on the experimental data and is a means for investigating the importance of individual terms in the equations of motion in addition to an order of magnitude analysis. This procedure also provides a means for quality comparison with other experimental data.

Law of the Wall Analysis

The following integral relation for a compressible law of the wall is obtained by applying Prandtl's mixing length approximation of the Reynolds stress and assuming that the mixing length, $l = Ky$

$$\frac{u_\infty}{u_\tau}\int_0^{u/u_\infty}\left(\frac{\rho}{\rho_w}\right)^{1/2} d\left(\frac{u}{u_\infty}\right) = u^{++} = \frac{1}{K}\log_e y^+ + C \qquad (12)$$

A compressible "law of the wall" and "law of the wake" can be formed using Eq. (12) by substituting values for K and C that have yielded good correlation of incompressible turbulent boundary-layer data. An expression linking the "wall law" and the "wake law" in the logarithmic region of overlap can be written as

$$u^{++} = 2.5\log_e y^+ + 5.1 + 2.5\Pi\omega(y/\delta) \qquad (13)$$

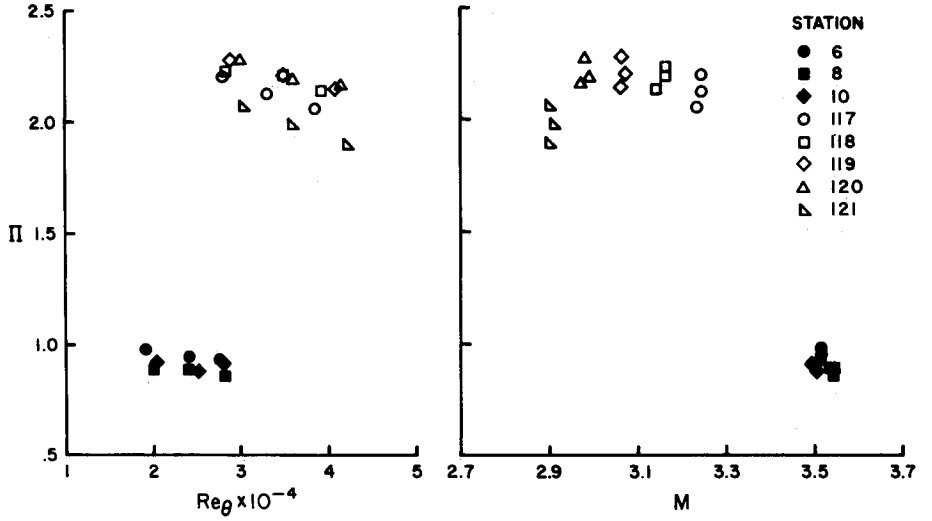

Fig. 6 Variation of Π with Re_θ and M.

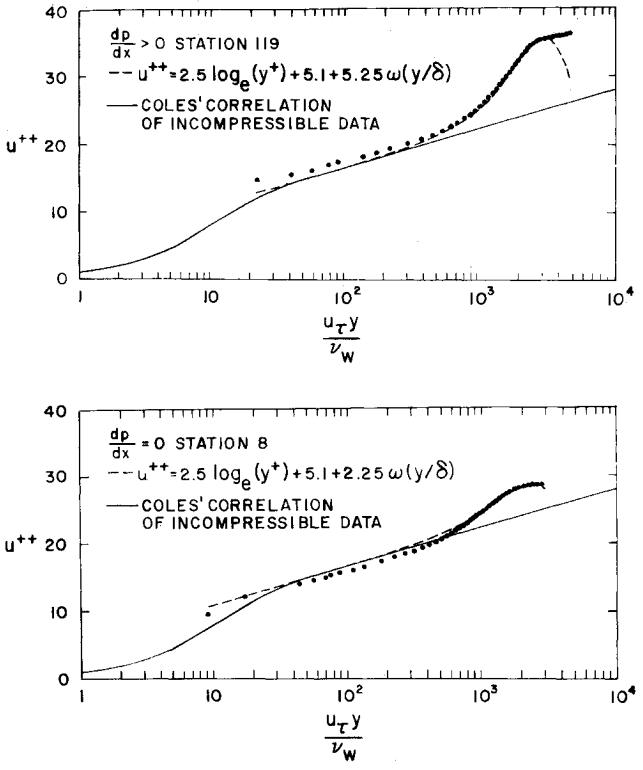

Fig. 7 Combined "wall law" and "wake law" data correlation.

where ω is Coles' wake function which can be approximated by $\omega = 2\sin^2(\pi y/2\delta)$ and Π is to be determined.

Values of Π have been determined from the experimental data using the relation

$$\Pi = 0.2(u_\delta^{++} - 2.5\log_e y_\delta^{+} - 5.1) \tag{14}$$

where u^{++} and y^{+} are evaluated at $y = \delta$. The values obtained are shown plotted versus Mach number and momentum thickness Reynolds number in Eig. 6.

The zero pressure gradient data show a slight tendency for Π to decrease with increasing Re_θ. The data for $dp/dx > 0$ exhibit the trends of Π decreasing with increasing M and decreasing with increasing Re_θ. The trend of Π decreasing with increasing M agrees with the trend indicated for the transformed variables of Baronti and Libby[3] who considered data for $dp/dx = 0$. However, the trend noted by Baronti and Libby of Π increasing with increasing Re_θ is opposite to that indicated by the adverse pressure gradient data of this experiment. The change in value of Π with M and Re_θ is insignificant compared to the change in value with the change in flow configuration. Since Π is considered to be constant for an "equilibrium" turbulent boundary layer, the change in Π along the ramp model (which is the same as the variation with M) can be considered to be a "relaxing" effect. Representative values of Π for $dp/dx = 0$ and $dp/dx > 0$ are 0.90 and 2.10, respectively. These values are both high compared to the value of 0.55 which has been found to yield good correlation of incompressible zero pressure gradient data for sufficiently high values of Re_θ.

Table 2 Streamwise integrated momentum (lbf-in./ft^2), Eq. (11)

Sta	T_1	$-T_2$	T_3	T_4	T_5	LHS	RHS
117	0	0	0	0	0	0	0
118	46.3	68.18	0.728	13.52	4.93	2.66	1.08
119	71.2	115.16	1.453	25.83	11.57	5.10	2.26
120	101.5	105.48	2.151	37.90	20.46	3.51	3.55
121	144.4	232.45	2.812	53.07	24.99	7.15	4.99

Examples of the correlation achieved using Eq. (13) are shown in Fig. 7. The slope of the logarithmic line agrees well with the experimental data; however, the value of 5.1 is too high for $dp/dx = 0$ and too low for $dp/dx > 0$. Values for this constant have been calculated using the relation

$$C = u^{++} - 2.5\log_e y^{+} \tag{15}$$

where u^{++} and y^{+} are evaluated at $y/\delta \approx 0.1$.

The values obtained for C are shown in Fig. 8 plotted vs M and Re_θ. The data for $dp/dx = 0$ show no dependence on Re_θ. The data for $dp/dx > 0$ tend to increase with increasing Re_θ and decreasing M. Representative values of C for $dp/dx = 0$ and $dp/dx > 0$ are 4.7 and 6.1, respectively.

This represents a small correction to the value of u^{++}. For instance at

$$y/\delta \approx 0.1, \qquad u^{++} \approx 18$$

hence $(6.1 - 5.1)/18 = 5.5\%$.

The uncertainty in C can also be accounted for by an uncertainty in the wall shear stress. As an example, it was found that increasing the wall shear stress by 10% resulted in agreement with the relation

$$u^{++} = 2.5\log_e y^{+} + 5.1$$

at $y/\delta \approx 0.1$ for a typical profile on the ramp model. This is comparable to the accuracy of the experimental determination of wall shear stress using the Preston tube technique.

Skin-Friction Measurements

The skin-friction data of this experiment are compared to the empirical correlation of Spalding and Chi[4] and to other experi-

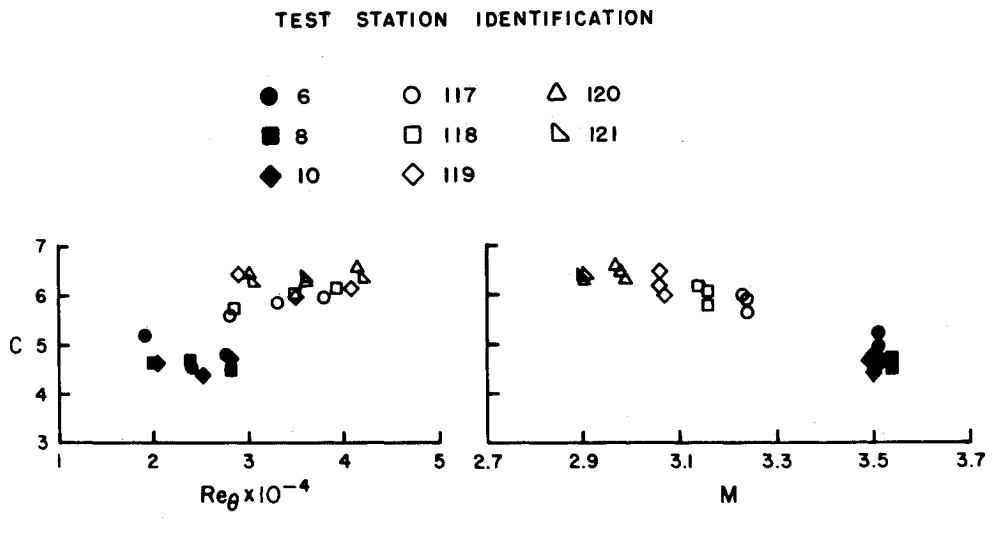

Fig. 8 Variation of C with Re_θ and M.

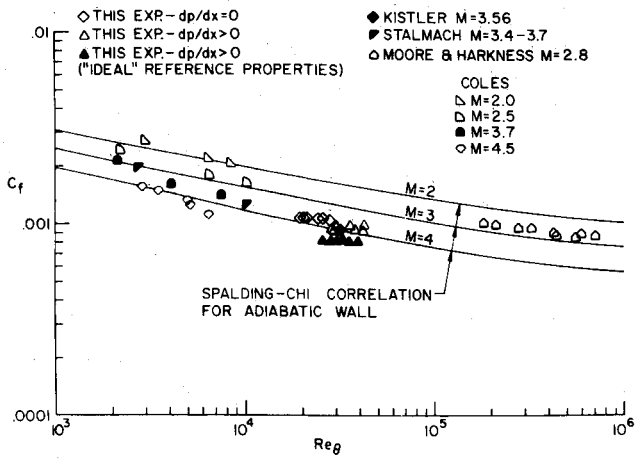

Fig. 9 Skin-friction data comparison.

mental measurements in Fig. 9. The skin-friction data of this experiment are approximately 8% and 35% low for the zero pressure gradient and adverse pressure gradient flow, respectively, compared to the correlation of Spalding and Chi. The data of this experiment compare more favorably with the data of Coles,[5] Stalmach,[6] and Kistler.[7]

The correlation of Spalding and Chi predicts a greater value of c_f in the region of adverse pressure gradient than in the region of zero pressure gradient. This is opposite to that indicated by the experimental data. The trend of the experimental c_f to increase in the streamwise direction for the flow over the ramp model is shown in Fig. 10 to agree with the trend predicted by the Spalding-Chi correlation although the increase in $c_{f,\,\mathrm{exp}}$ is less. Comparing the trend of $c_{f,\,\mathrm{exp}}$ to the predicted trend, it is seen that the effect of concave longitudinal curvature is to decrease the local skin-friction coefficient compared to what it would be for a flat plate at the same value of Mach number and momentum thickness Reynolds number.

Integral Properties for Flow with Significant Static Pressure Variation Normal to the Surface

Conventional definitions of the integral properties of the boundary layer must be modified when considering flows with significant static pressure variation through the boundary layer due to the lack of a freestream region with constant properties. The need to modify conventional definitions of the integral properties has been recognized by other researchers,[9-11] but no agreement as to the best interpretation has been reached.

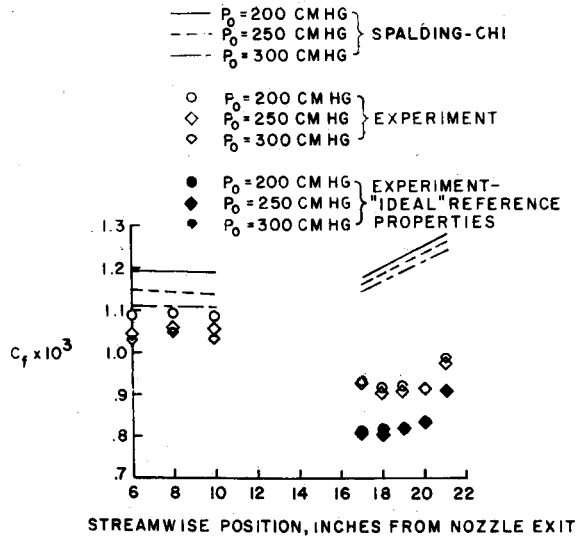

Fig. 10 Skin friction vs streamwise position.

The integral properties are defined here by considering the flux deficit appearing within the boundary layer referenced to "ideal" properties calculated using the experimentally determined static pressure profile. The integral thicknesses are referenced to the ideal properties at the wall. These definitions reduce to the classical definitions of the integral properties for the case of constant static pressure through the boundary layer. The integral properties according to this interpretation are

displacement thickness

$$\rho_w' u_w' \delta^{*\prime} = \int_0^\infty (\rho' u' - \rho u)\, dy \tag{16}$$

momentum thickness

$$\rho_w' u_w'^2 \theta' = \int_0^\infty \rho u (u' - u)\, dy \tag{17}$$

energy thickness

$$\rho_w' u_w'^3 \theta_E' = \int_0^\infty \rho u (u'^2 - u^2)\, dy \tag{18}$$

velocity thickness

$$u_w' \delta_u' = \int_0^\infty (u' - u)\, dy \tag{19}$$

enthalpy thickness

$$c_p \rho_w' u_w' T_w' \theta_H' = \int_0^\infty c_p \rho u (T - T')\, dy \tag{20}$$

where the ideal properties ρ', u', T' are calculated from the measured static pressure profile assuming constant total temperature equal to the value in the freestream and constant total pressure equal to the tunnel total pressure. The integral properties according to this interpretation are illustrated in Fig. 11. The profiles in Fig. 11 were formed using the experimental data and accurately represent the measured flux of the quantity indicated. The definitions given above for $\delta^{*\prime}$ and θ' are identical to those of McLafferty and Barber.[9] The only difference is that McLafferty and Barber inferred a static pressure profile from measurements of tunnel total pressure, impact pressure and wall pressure while measured values of static pressure are used here. An important

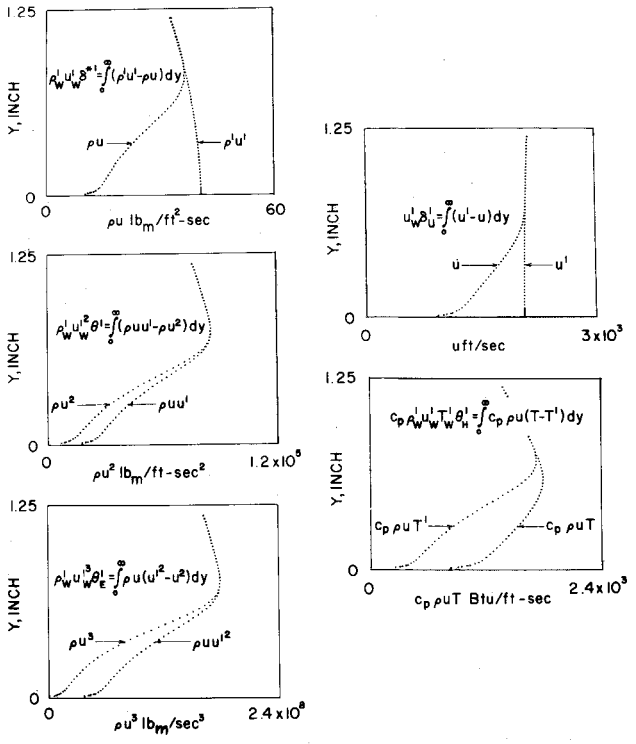

Fig. 11 Integral thicknesses defined using reference properties calculated assuming $p_{t_1} = p_o$ and $T_t = T_{t\infty}$.

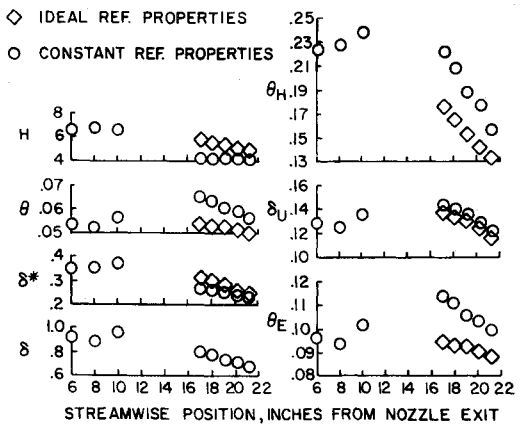

Fig. 12 Integral properties and boundary-layer thickness vs streamwise position.

feature of this definition is that the integral thickness does not depend upon the value chosen for the boundary-layer thickness since the inviscid properties become identical to the actual properties near the edge of the boundary layer.

The integral thicknesses were calculated in two ways for the adverse pressure gradient data: 1) using the calculated "ideal" properties for reference as discussed above, and 2) using measured values of density and velocity at the position of maximum mass flux for the reference values. The integral thicknesses are compared in Fig. 12. The boundary-layer thickness δ is the position of maximum mass flux for the adverse pressure gradient profiles and the position for $u = 0.995u_\infty$ for the zero pressure gradient profiles.

It is seen that $d\delta^*/dx$ has a steeper slope than $d\delta^*/dx$. In contrast, the slope of $d\theta/dx$ is steeper than $d\theta'/dx$. The shape factor H' changes considerably along the ramp model while H changes but slightly. The velocity thickness is the only integral property that does not exhibit significantly different behavior for the two methods of calculation. These results indicate that calculation procedures employing integral relations can yield questionable results when regions of significant static pressure variation normal to the surface are encountered.

Conclusions

An experimental investigation of the supersonic turbulent boundary layer in a region of moderate adverse pressure gradient created by a two-dimensional isentropic ramp model has been conducted at a Mach number of 3.5 for a closely adiabatic wall with values of momentum thickness Reynolds number ranging from 1.9 to 4.2×10^4. All the parameters needed to enable calculation of a complete set of mean profile characteristics have been measured. Analysis of the experimental data has led to the following conclusions:

1) Corrections for longitudinal curvature to the equation for conservation of streamwise momentum represent small corrections to the individual terms involved; but the corrections are of the same order of magnitude as the contribution of the wall shear stress.

2) The conservation of momentum in the direction normal to the surface is adequately represented by the balance of centrifugal force by the normal pressure gradient.

3) The integral compressibility transformation defined by Eq. (12) yields good correlation of the experimental data with the "law of the wall" written using values of the "universal" constants that have given good correlation of incompressible turbulent boundary-layer data.

4) The value of the skin-friction coefficient for the flow over the ramp model is 20% less than that for the zero pressure gradient flow immediately upstream of the ramp model.

5) For the conditions of this experiment, the increase in skin-friction coefficient along a surface with concave longitudinal curvature is less than would be predicted for a zero pressure gradient flow along a flat plate with identical values of Re_θ, M, and T_w/T_∞. Further details of the analysis of the experimental data are available in Refs. 12 and 13.

References

[1] Sturek, W. B. and Danberg, J. E., "The Supersonic Turbulent Boundary Layer in Adverse Pressure Gradient. Part I: The Experiment," *AIAA Journal*, Vol. 10, No. 4, April 1972, pp. 475–480.

[2] Tetervin, Neal, "An Exploratory Theoretical Investigation of the Effect of Longitudinal Surface Curvature on the Turbulent Boundary Layer," NOL-TR 69-22, Feb. 1969, Naval Ordnance Lab., White Oak, Md.

[3] Baronti, P. O. and Libby, P. A., "Velocity Profiles in Turbulent Compressible Boundary Layers," *AIAA Journal*, Vol. 4, No. 2, Feb. 1966, pp. 193–202.

[4] Spalding, D. B. and Chi, S. W., "The Drag of a Compressible Turbulent Boundary Layer on a Smooth Flate Plate With and Without Heat Transfer," *Journal of Fluid Mechanics*, Vol. 18, Pt. I, Jan. 1964, pp. 117–143.

[5] Coles, Donald E., "Measurements in the Boundary Layer on a Smooth Flat Plate in Supersonic Flow. III. Measurements in a Flat-Plate Boundary Layer at the Jet Propulsion Laboratory," Rept. 20-71, June 1953, Jet Propulsion Lab., Pasadena, Calif.

[6] Stalmach, C. J., Jr., "Experimental Investigations of the Surface Impact Probe Method of Measuring Local Skin Friction at Supersonic Speeds," DRL-410, Jan. 1958, Univ. of Texas Defense Research Lab., Austin, Texas.

[7] Kristler, A. L., "Fluctuation Measurements in Supersonic Turbulent Boundary Layers," BRL R 1052, Aug. 1958, Ballistic Research Lab., Aberdeen Proving Ground, Md.

[8] Moore, D. R. and Harkness, J., "Experimental Investigations of the Compressible Turbulent Boundary Layer at Very High Reynolds Numbers," *AIAA Journal*, Vol. 3, No. 4, April 1965, pp. 631–638.

[9] McLafferty, G. H. and Barber, R. E., "The Effect of Adverse Pressure Gradient on the Characteristics of Turbulent Boundary Layers in Supersonic Streams," *Journal of the Aerospace Sciences*, Vol. 29, No. 1, Jan. 1962, pp. 1–10.

[10] Kepler, C. E. and O'Brien, R. L., "Supersonic Turbulent Boundary Layer Growth Over Cooled Walls in Adverse Pressure Gradients," Tech. Documentary Rept. ASD TDR 62-87, Oct. 1962, Air Force Systems Command, Wright-Patterson Air Force Base, Ohio.

[11] Hoydysh, W. G. and Zakkay, V., "An Experimental Investigation of Hypersonic Turbulent Boundary Layers in Adverse Pressure Gradient," *AIAA Journal*, Vol. 7, No. 1, Jan. 1969, pp. 105–116.

[12] Sturek, W. B., "The Supersonic Turbulent Boundary Layer in a Moderate Adverse Pressure Gradient. Part II. Analysis of the Experimental Data," BRL R 1543, AD 729325, June 1971, Ballistic Research Lab., Aberdeen Proving Ground, Md.

[13] Sturek, W. B., Ph.D. dissertation, June 1971, Univ. of Delaware, Newark, Del.